

Observation of the decays $B^+ \rightarrow \Sigma_c(2455)^{++}\bar{\Xi}_c^-$ and $B^0 \rightarrow \Sigma_c(2455)^0\bar{\Xi}_c^0$

M. Abumusabh , I. Adachi , L. Aggarwal , H. Ahmed , Y. Ahn , H. Aihara , N. Akopov , S. Alghamdi , M. Alhakami , A. Aloisio , N. Althubiti , K. Amos , N. Anh Ky , D. M. Asner , H. Atmacan , T. Aushev , V. Aushev , R. Ayad , V. Babu , H. Bae , N. K. Baghel , S. Bahinipati , P. Bambade , Sw. Banerjee , M. Barrett , M. Bartl , J. Baudot , A. Baur , A. Beaubien , F. Becherer , J. Becker , J. V. Bennett , F. U. Bernlochner , V. Bertacchi , M. Bertemes , E. Bertholet , M. Bessner , S. Bettarini , V. Bhardwaj , B. Bhuyan , F. Bianchi , D. Biswas , A. Bobrov , D. Bodrov , A. Bondar , G. Bonvicini , J. Borah , A. Boschetti , A. Bozek , M. Bračko , P. Branchini , R. A. Briere , T. E. Browder , A. Budano , S. Bussino , Q. Campagna , M. Campajola , L. Cao , G. Casarosa , C. Cecchi , M.-C. Chang , P. Cheema , L. Chen , B. G. Cheon , K. Chilikin , J. Chin , K. Chirapatpimol , H.-E. Cho , K. Cho , S.-J. Cho , S.-K. Choi , S. Choudhury , L. Corona , J. X. Cui , E. De La Cruz-Burelo , S. A. De La Motte , G. De Nardo , G. De Pietro , R. de Sangro , M. Destefanis , S. Dey , A. Di Canto , J. Dingfelder , Z. Doležal , I. Domínguez Jiménez , T. V. Dong , X. Dong , M. Dorigo , K. Dugic , G. Dujany , P. Ecker , D. Epifanov , J. Eppelt , R. Farkas , P. Feichtinger , T. Ferber , T. Fillinger , C. Finck , G. Finocchiaro , F. Forti , A. Frey , B. G. Fulsom , A. Gabrielli , A. Gale , E. Ganiev , M. Garcia-Hernandez , R. Garg , G. Gaudino , V. Gaur , V. Gautam , A. Gellrich , D. Ghosh , H. Ghumaryan , G. Giakoustidis , R. Giordano , A. Giri , P. Gironella Gironell , B. Gobbo , R. Godang , P. Goldenzweig , W. Gradl , E. Graziani , D. Greenwald , K. Gudkova , I. Haide , Y. Han , C. Harris , H. Hayashii , S. Hazra , C. Hearty , M. T. Hedges , G. Heine , I. Heredia de la Cruz , T. Higuchi , M. Hoek , M. Hohmann , R. Hoppe , P. Horak , X. T. Hou , C.-L. Hsu , T. Humair , T. Iijima , K. Inami , N. Ipsita , A. Ishikawa , R. Itoh , M. Iwasaki , P. Jackson , W. W. Jacobs , E.-J. Jang , Q. P. Ji , Y. Jin , A. Johnson , J. Kandra , K. H. Kang , F. Keil , C. Kiesling , C.-H. Kim , D. Y. Kim , J.-Y. Kim , K.-H. Kim , Y.-K. Kim , H. Kindo , K. Kinoshita , P. Kodyš , T. Koga , S. Kohani , K. Kojima , A. Korobov , S. Korpar , E. Kovalenko , R. Kowalewski , P. Krizan , P. Krokovny , T. Kuhr , Y. Kullii , R. Kumar , K. Kumara , T. Kunigo , A. Kuzmin , Y.-J. Kwon , K. Lalwani , T. Lam , J. S. Lange , T. S. Lau , M. Laurenza , R. Lebourder , F. R. Le Diberder , M. J. Lee , C. Lemettais , P. Leo , P. M. Lewis , C. Li , H.-J. Li , L. K. Li , Q. M. Li , W. Z. Li , Y. Li , Y. B. Li , Y. P. Liao , J. Libby , J. Lin , V. Lisovskyi , M. H. Liu , Q. Y. Liu , Z. Liu , D. Liventsev , S. Longo , A. Lozar , T. Lueck , C. Lyu , Y. Ma , M. Maggiora , S. P. Maharana , R. Maiti , G. Mancinelli , R. Manfredi , E. Manoni , M. Mantovano , D. Marcantonio , S. Marcello , C. Marinas , C. Martellini , A. Martens , T. Martinov , L. Massaccesi , M. Masuda , T. Matsuda , D. Matvienko , S. K. Maurya , M. Maushart , J. A. McKenna , Z. Medankin Gruberová , R. Mehta , F. Meier , D. Meleshko , M. Merola , C. Miller , M. Mirra , K. Miyabayashi , H. Miyake , S. Mondal , S. Moneta , A. L. Moreira de Carvalho , H.-G. Moser , R. Mussa , I. Nakamura , M. Nakao , H. Nakazawa , Y. Nakazawa , M. Naruki , Z. Natkaniec , A. Natchii , M. Nayak , M. Neu , S. Nishida , S. Ogawa , R. Okubo , H. Ono , Y. Onuki , G. Pakhlova , S. Pardi , J. Park , S.-H. Park , B. Paschen , S. Patra , S. Paul , T. K. Pedlar , R. Pestotnik , L. E. Piilonen , P. L. M. Podesta-Lerma , T. Podobnik , C. Praz , S. Prell , E. Prencipe , M. T. Prim , S. Privalov , H. Purwar , P. Rados , G. Raeuber , S. Raiz , V. Raj , K. Ravindran , J. U. Rehman , M. Reif , S. Reiter , D. Ricalde Herrmann , I. Ripp-Baudot , G. Rizzo , S. H. Robertson , J. M. Roney , A. Rostomyan , N. Rout , D. A. Sanders , S. Sandilya , L. Santelj , C. Santos , V. Savinov , B. Scavino , G. Schnell , M. Schnepf , K. Schoenning , C. Schwanda , Y. Seino , A. Selce , K. Senyo , J. Serrano , C. Sfienti , W. Shan , G. Sharma , C. P. Shen , X. D. Shi , T. Shillington , T. Shimasaki , J.-G. Shiu , D. Shtol , B. Shwartz , A. Sibidanov , F. Simon , J. B. Singh , J. Skorupa , R. J. Sobie , M. Sobotzik , A. Soffer , A. Sokolov , E. Solovieva , S. Spataro , B. Spruck , M. Starič , P. Stavroulakis , L. Stoetzer , R. Stroili <

(The Belle and Belle II Collaborations)

We report the first observation of the two-body baryonic decays $B^+ \rightarrow \Sigma_c(2455)^{++}\bar{\Xi}_c^-$ and $B^0 \rightarrow \Sigma_c(2455)^0\bar{\Xi}_c^0$ with significances of 7.3σ and 6.2σ , respectively, including statistical and systematic uncertainties. The branching fractions are measured to be $\mathcal{B}(B^+ \rightarrow \Sigma_c(2455)^{++}\bar{\Xi}_c^-) = (5.74 \pm 1.11 \pm 0.42^{+2.47}_{-1.53}) \times 10^{-4}$ and $\mathcal{B}(B^0 \rightarrow \Sigma_c(2455)^0\bar{\Xi}_c^0) = (4.83 \pm 1.12 \pm 0.37^{+0.72}_{-0.60}) \times 10^{-4}$. The first and second uncertainties are statistical and systematic, respectively, while the third ones arise from the absolute branching fractions of $\bar{\Xi}_c^-$ or $\bar{\Xi}_c^0$ decays. The data samples used for this analysis have integrated luminosities of 711 fb^{-1} and 365 fb^{-1} , and were collected at the $\Upsilon(4S)$ resonance by the Belle and Belle II detectors operating at the KEKB and SuperKEKB asymmetric-energy e^+e^- colliders, respectively.

Baryonic B decays provide an important dynamical system for studying the production mechanisms of baryon-antibaryon pairs in the nonperturbative regime of quantum chromodynamics (QCD). Over the past three decades, a number of such decays have been observed [1] that have many interesting features, such as threshold enhancements in the baryon-antibaryon mass spectra [2–5] and a hierarchy in the branching fractions between two-body and multi-body decays [6, 7]. These observations help elucidate the intricate kinematic and dynamical properties of baryonic B decays [8].

In 2003, the Belle experiment reported the first observation of a two-body baryonic decay, and measured the decay $B^0 \rightarrow \bar{\Lambda}_c^- p$ to have a branching fraction of order 10^{-5} [9]. In 2006, Belle observed the double-charm decays $B \rightarrow \Lambda_c^+ \bar{\Xi}_c^-$ [10]; this result was later confirmed by the BaBar experiment [11]. The double-charm decays have branching fractions of order 10^{-3} . The decays $B^0 \rightarrow \bar{\Lambda}_c^- p$ and $B \rightarrow \Lambda_c^+ \bar{\Xi}_c^-$, which proceed via the quark-level transitions $b \rightarrow c\bar{d}\bar{u}$ and $b \rightarrow c\bar{s}\bar{c}$, respectively, involve combinations of Cabibbo–Kobayashi–Maskawa (CKM) matrix elements of comparable magnitudes [12]. Nevertheless, their branching fractions differ by nearly two orders of magnitude, suggesting that certain mechanisms may enhance or suppress specific processes. Several possible mechanisms have been proposed to account for the large decay rates into pairs of charmed baryons, including σ/π meson exchange via soft nonperturbative interactions [13, 14], final-state interactions [15], and hard gluon exchange [16]. Further measurements of B decays into charmed baryon pairs are useful for probing the underlying dynamics and discriminating among different theoretical mechanisms.

Theoretical studies of the $B^+ \rightarrow \Sigma_c(2455)^{++}\bar{\Xi}_c^-$ and $B^0 \rightarrow \Sigma_c(2455)^0\bar{\Xi}_c^0$ decays use a QCD sum rule [17] and the diquark model [18]. The QCD sum rule predicted these double-charm branching fractions to be as large as 4×10^{-3} [17], while the diquark model estimated them to be of the order 10^{-4} , or 30%–70% of those of the $B^+ \rightarrow \Lambda_c^+ \bar{\Xi}_c^0$ and $B^0 \rightarrow \Lambda_c^+ \bar{\Xi}_c^-$ decays [18]. These two decays proceed through a purely internal W -boson emission amplitude [19], as shown in Fig. 1. This topology gives rise to a nonfactorizable amplitude [20], stemming from

the nonperturbative QCD dynamics such as final-state interactions and soft gluon exchanges [21–24]. These two decay modes thus provide a theoretically reliable environment to probe such effects. In addition, according to $SU(3)$ flavor symmetry, the $\Sigma_c(2455)$ baryon belongs to a sextet of flavor-symmetric states, while the $\bar{\Xi}_c$ baryon belongs to an antitriplet of flavor-antisymmetric states. To date, no B decays into charmed baryon pairs containing both an antitriplet and a sextet have been observed.

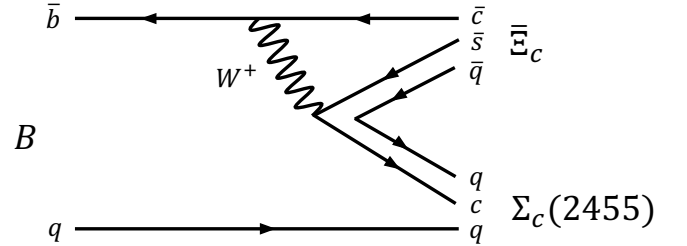


FIG. 1: Diagram representing the internal W -boson emission amplitude for the decays $B^+ \rightarrow \Sigma_c(2455)^{++}\bar{\Xi}_c^-$ and $B^0 \rightarrow \Sigma_c(2455)^0\bar{\Xi}_c^0$, corresponding to $q = u$ and $q = d$, respectively.

We report the first search for the decays $B^+ \rightarrow \Sigma_c(2455)^{++}\bar{\Xi}_c^-$ and $B^0 \rightarrow \Sigma_c(2455)^0\bar{\Xi}_c^0$. Charge-conjugate channels are implicitly included throughout this analysis. This study is based on data samples that have integrated luminosities of 711 fb^{-1} [25], collected by the Belle detector [26], and 365 fb^{-1} [27], collected by the Belle II detector [28], at the e^+e^- center-of-mass (c.m.) energy (\sqrt{s}) of 10.58 GeV. The data sets contain $(772 \pm 11) \times 10^6$ $\Upsilon(4S)$ events for Belle and $(387 \pm 6) \times 10^6$ $\Upsilon(4S)$ events for Belle II. The $\Sigma_c(2455)^{+,0}$ baryons are reconstructed in their $\Lambda_c^+ \pi^\pm$ decays followed by the $\Lambda_c^+ \rightarrow pK^-\pi^+$ and $\Lambda_c^+ \rightarrow pK_S^0$ decays. The $\bar{\Xi}_c^-$ baryon is reconstructed via $\bar{\Xi}_c^- \rightarrow \bar{\Xi}^+ \pi^-\pi^-$ and $\bar{p}K^+\pi^-$ decays, and the $\bar{\Xi}_c^0$ baryon via $\bar{\Xi}_c^0 \rightarrow \bar{\Xi}^+ \pi^-$ and $\bar{\Lambda}K^+\pi^-$ decays, followed by $\bar{\Xi}^+ \rightarrow \bar{\Lambda}\pi^+$. To avoid experimental bias, the signal region is not examined until the analysis procedure is finalized. All selection criteria are determined by iteratively optimizing the figure-of-merit for an observation at a significance level of five standard deviations based on simulation [29]. The signal

yields are extracted from a two-dimensional (2D) fit to the distributions of the difference between the expected and observed B meson energy and the $\Lambda_c^+ \pi$ invariant mass. The 2D fit is performed simultaneously on events from the signal and sideband regions of the Ξ_c^- invariant mass.

The Belle detector operated at the KEKB [30] asymmetric-energy e^+e^- collider, while the Belle II detector operates at its successor, the SuperKEKB collider [31]. The two detectors are nearly 4π hermetic solenoidal magnetic spectrometers. They both consist of an inner silicon vertex detector and a central drift chamber, surrounded by Cherenkov-based charged-particle identification detectors, a crystal electromagnetic calorimeter, and outer detectors for muon and K_L^0 meson identification via penetration depth. Detailed descriptions of the Belle and Belle II detectors can be found in Refs. [26, 28].

Monte Carlo (MC) simulated signal events are used to optimize the selection criteria, calculate the reconstruction efficiencies, and determine the fit models. The EVTGEN [32] and PYTHIA [33, 34] software packages are used to generate $e^+e^- \rightarrow \Upsilon(4S) \rightarrow B\bar{B}$ with final-state radiation simulated by the PHOTOS software package [35]. In the simulation, one B meson decays inclusively, while the other decays into a signal mode. Inclusive simulated samples of $e^+e^- \rightarrow q\bar{q}$, where q indicates a u , d , s , or c quark, and $\Upsilon(4S) \rightarrow B\bar{B}$ are used to optimize the selection criteria and identify the background sources [36]. The KKMC [37] and PYTHIA [33, 34] software packages are used to simulate the $e^+e^- \rightarrow q\bar{q}$ processes. The detector responses are modeled by the software packages GEANT3 [38] for Belle and GEANT4 [39] for Belle II.

We use the Belle II analysis software framework (basf2) [40, 41], a modular software toolkit developed for Belle II data processing, to reconstruct both Belle and Belle II data. The Belle data are converted into a basf2-compatible format using the B2BII (Belle-to-Belle II) package [42], enabling a unified analysis workflow across the two experiments. The hardware trigger, which relies on total energy and neutral-particle multiplicity, is optimized to select hadronic events and is fully efficient for the signal modes. In the offline analysis, the distance of closest approach to the interaction point for charged-particle trajectories (tracks) is required to be less than 2.0 cm in the plane perpendicular to the z axis and less than 4.0 cm parallel to it, except for the K_S^0 , $\bar{\Lambda}$, and Ξ^+ decay products. The z axis is the solenoid axis, with positive direction along the e^- beam, common to both Belle and Belle II. The identification of charged tracks uses the likelihood ratio $\mathcal{R}(h|h') = \mathcal{L}(h)/[\mathcal{L}(h) + \mathcal{L}(h')]$, where $\mathcal{L}(h^{(\prime)})$ is the likelihood of the charged track being a hadron $h^{(\prime)} = p, K$, or π . This likelihood ratio is determined using a particle identification (PID) algorithm that integrates information from the Belle and Belle II subdetectors [43, 44]. Tracks with

$\mathcal{R}(p|K) > 0.6$ and $\mathcal{R}(p|\pi) > 0.6$ are identified as proton candidates; charged kaon (pion) candidates must satisfy $\mathcal{R}(K|\pi) > 0.6$ (< 0.4). The efficiencies of these PID requirements range from 85% to 94%, with corresponding misidentification rates between 3% and 8%. We omit PID requirements for the pion candidates used to reconstruct K_S^0 , $\bar{\Lambda}$, and Ξ^+ candidates, as their kinematic properties provide sufficient discrimination.

The K_S^0 candidates are first reconstructed from pairs of oppositely charged particles assumed to be pions with a common vertex, and then selected using a neural network in Belle [45] and a boosted decision tree in Belle II [46]. Both discriminators primarily rely on the kinematic information of K_S^0 and its decay products. The invariant mass of K_S^0 candidates is required to be within $9.0 \text{ MeV}/c^2$ of its known mass [1], corresponding to approximately 2.5 times the mass resolution (σ). The $\bar{\Lambda}$ candidates are reconstructed from $\bar{p}\pi^+$ pairs with a common vertex, and an invariant mass within $5.5 \text{ MeV}/c^2$ of its mass [1] (approximately 2.5σ). The selected $\bar{\Lambda}$ candidate is then combined with a π^+ to form a Ξ^+ candidate. The invariant mass of Ξ^+ candidates is required to be within $6.5 \text{ MeV}/c^2$ of its mass [1] (approximately 2.5σ).

The invariant masses of the Λ_c^+ , Ξ_c^- , and Ξ_c^0 charmed baryon candidates are required to lie within 15.0, 18.0, and 18.0 MeV/c^2 of their known values [1], respectively, corresponding to mass ranges of approximately 2.5σ . The selected Λ_c^+ candidates are combined with π^\pm candidates to form $\Sigma_c(2455)^{+,0}$ candidates, which are subsequently combined with $\Xi_c^{-,0}$ candidates to reconstruct $B^{+,0}$ candidates. Each signal channel thus has four distinct reconstruction modes. For each of the intermediate particle candidates (K_S^0 , $\bar{\Lambda}$, Ξ^+ , Λ_c^+ , $\Sigma_c(2455)^{+,0}$, and $\Xi_c^{-,0}$), the tracks associated with its decay products are fitted to a common vertex, and the invariant mass is constrained to the corresponding known value [1]. A vertex fit is applied to the $B^{+,0}$ candidates. When reconstructing modes involving $\Xi_c^- \rightarrow \bar{p}K^+\pi^-$ decays, a requirement of $\chi^2/\text{ndf} < 10$ on the B^+ vertex fit is imposed to further suppress combinatorial background, where ndf is the number of degrees of freedom. If multiple candidates are present in an event, all combinations are retained for further analysis. The fraction of events with multiple candidates ranges from 3% to 5% in data, in agreement with expectations from simulation. The average number of candidates in such events is between 2.02 and 2.06, with misreconstructed candidates contributing as smooth background.

Backgrounds are studied using both inclusive MC samples and data from the sideband regions of the $M(\Lambda_c^+)$, $M(\Xi_c^{-,0})$, and M_{bc} distributions. The $M(\Lambda_c^+)$ and $M(\Xi_c^{-,0})$ denote the invariant masses of the reconstructed Λ_c^+ and $\Xi_c^{-,0}$ candidates, and the M_{bc} is defined as $M_{bc} = \sqrt{E_{\text{beam}}^2 - (\sum_i \vec{p}_i)^2}$, where $E_{\text{beam}} =$

$\sqrt{s}/2$ is the beam energy in the e^+e^- c.m. system, and \vec{p}_i is the momentum of the i th daughter of the B meson. We require $M_{bc} > 5.27$ GeV/ c^2 , which retains more than 97% of the signal. The sideband regions of $M(\Lambda_c^+)$, $M(\Xi_c^{-,0})$, and M_{bc} are $2231.0 < M(\Lambda_c^+) < 2261.0$ MeV/ c^2 or $2311.0 < M(\Lambda_c^+) < 2341.0$ MeV/ c^2 , $2398.0 < M(\Xi_c^{-,0}) < 2434.0$ MeV/ c^2 or $2504.0 < M(\Xi_c^{-,0}) < 2540.0$ MeV/ c^2 , and $5.235 < M_{bc} < 5.265$ GeV/ c^2 , respectively, which are twice as wide as the corresponding signal region. The corresponding $M(\Lambda_c^+\pi^\pm)$ and ΔE distributions from these sideband regions in the combined Belle and Belle II data samples are presented in the supplemental material [47]. Here and throughout, $M(\Lambda_c^+\pi^\pm)$ is the invariant mass of the $\Sigma_c(2455)^{+,0}$ candidate, and ΔE is defined as $\Delta E = \sum_i E_i - E_{\text{beam}}$, where E_i is the energy of the i th daughter of the B meson in the e^+e^- c.m. frame. The $M(\Lambda_c^+)$ and M_{bc} sideband events have no significant peaks in either the $M(\Lambda_c^+\pi^\pm)$ or ΔE distributions, while the $M(\Xi_c^{-,0})$ sideband events contain small potential peaks in both distributions.

To extract the signal yields, we perform a 2D extended maximum likelihood fit to the unbinned $M(\Lambda_c^+\pi^\pm)$ and ΔE distributions, simultaneously using four data sets: events from the signal and sideband regions of $M(\Xi_c^{-,0})$ in both Belle and Belle II data. The fitting functions used to model events in the signal and sideband regions of $M(\Xi_c^{-,0})$ are parameterized as

$$f_1(M, \Delta E) = (N_{ss}^{\text{sig}} + 0.5N_{ss}^{\text{sbld}})s_1(M)s_2(\Delta E) \\ + N_{sb}^{\text{bg}}s_1(M)b_2(\Delta E) + N_{bs}^{\text{bg}}b_1(M)s_2(\Delta E) \\ + N_{bb}^{\text{bg}}b_1(M)b_2(\Delta E)$$

and

$$f_2(M, \Delta E) = N_{ss}^{\text{sbld}}s_1(M)s_2(\Delta E) + N_{sb}^{\text{sbld}}s_1(M)b_2'(\Delta E) \\ + N_{bs}^{\text{sbld}}b_1'(M)s_2(\Delta E) + N_{bb}^{\text{sbld}}b_1'(M)b_2'(\Delta E),$$

respectively. Here, $s_1(M)$ and $s_2(\Delta E)$ denote the signal probability density functions (PDFs) for the $M(\Lambda_c^+\pi^\pm)$ and ΔE distributions, respectively, while $b_1^{(\prime)}(M)$ and $b_2^{(\prime)}(\Delta E)$ represent the corresponding background PDFs. The factor of 0.5 in $f_1(M, \Delta E)$ arises from the ratio between the defined signal and sideband regions of $M(\Xi_c^{-,0})$, as the backgrounds are found to be linear. A Breit-Wigner function convolved with a Crystal-Ball function is used for $s_1(M)$, while a double-Gaussian function with two different mean values is employed for $s_2(\Delta E)$. The width of the Breit-Wigner function is fixed to the known intrinsic width of the $\Sigma_c(2455)^{+,0}$ [1], while the other parameters of $s_1(M)$ and $s_2(\Delta E)$ are fixed to the values obtained from fits to the corresponding simulated signal distributions. The background components $b_1^{(\prime)}(M)$ and $b_2^{(\prime)}(\Delta E)$ are modeled by first-order polynomials with free parameters. The signal PDFs for the sideband events are the same as

those used in the signal region. The peaking backgrounds are due to inclusive $B^{+,0} \rightarrow \Sigma_c(2455)^{+,0}X$ decays, where X denotes non- $\Xi_c^{-,0}$ final states, and contribute to both signal and $M(\Xi_c^{-,0})$ sideband regions. The number of signal events is denoted by N_{ss}^{sig} , the number of peaking background events by N_{ss}^{sbld} , and the number of combinatorial background events in both distributions by $N_{bb}^{\text{bg, sbld}}$. The yields of background contributions that peak in one distribution but not in the other are denoted by $N_{sb}^{\text{bg, sbld}}$ and $N_{bs}^{\text{bg, sbld}}$, corresponding to events that peak in the $M(\Lambda_c^+\pi^\pm)$ and ΔE distributions, respectively. All event yields are free parameters in the fit, with the signal yields in the Belle and Belle II data sets constrained according to the expected ratio for a common branching fraction.

Figure 2 shows the $M(\Lambda_c^+\pi^\pm)$ and ΔE distributions for events from the $M(\Xi_c^{-,0})$ signal region in the combined Belle and Belle II data. Each distribution is projected within the other's signal region, with fit results overlaid. The signal regions for $M(\Lambda_c^+\pi^\pm)$ and ΔE are defined as $2446.0 < M(\Lambda_c^+\pi^\pm) < 2464.0$ MeV/ c^2 and $|\Delta E| < 16$ MeV, respectively, which retain more than 95% of the signal. The fitted yields of peaking backgrounds in the signal region, shown as the cyan components, are 2.4 ± 3.5 and 2.0 ± 2.2 for the B^+ and B^0 channels, respectively. The corresponding fit results for events from these sideband regions are shown in the supplemental material [47]. The fitted signal yields for the decays $B^+ \rightarrow \Sigma_c(2455)^{++}\Xi_c^-$ and $B^0 \rightarrow \Sigma_c(2455)^0\Xi_c^-$ are 52.8 ± 10.2 and 31.1 ± 7.2 , respectively, with statistical significances of 7.8σ and 6.7σ . These significances are calculated using $\sqrt{-2\ln(\mathcal{L}_0/\mathcal{L}_{\text{max}})}$, where \mathcal{L}_0 and \mathcal{L}_{max} are the values of the likelihoods maximized without and with the signal component, respectively. To estimate the signal significances accounting for systematic uncertainties, several alternative fits are performed: (1) the background components $b_1(M)$ and $b_2(\Delta E)$ are modeled using either second-order polynomials or exponential functions; (2) the fixed signal shapes $s_1(M)$ and $s_2(\Delta E)$ are convolved with Gaussian functions that have floating resolutions; (3) the fixed width of the $\Sigma_c(2455)^{+,0}$ is varied by $\pm 1\sigma$ [1]; (4) the sideband regions of $M(\Xi_c^{-,0})$ are shifted by ± 10 MeV/ c^2 . Across all fit variations, the observed signal significances exceed 7.3σ for the $B^+ \rightarrow \Sigma_c(2455)^{++}\Xi_c^-$ decay and 6.2σ for the $B^0 \rightarrow \Sigma_c(2455)^0\Xi_c^-$ decay. These values are taken as the final signal significances after incorporating systematic effects.

The branching fractions of the $B^+ \rightarrow \Sigma_c(2455)^{++}\Xi_c^-$ and $B^0 \rightarrow \Sigma_c(2455)^0\Xi_c^-$ decays are calculated using

$$\mathcal{B} = \frac{N_{ss}^{\text{sig}}}{2f_x[N_{\Upsilon(4S)}^{\text{b1}} \sum_i (\epsilon_i^{\text{b1}} \mathcal{B}_i) + N_{\Upsilon(4S)}^{\text{b2}} \sum_i (\epsilon_i^{\text{b2}} \mathcal{B}_i)]}.$$

Here, N_{ss}^{sig} represents the number of fitted $B^+ \rightarrow$

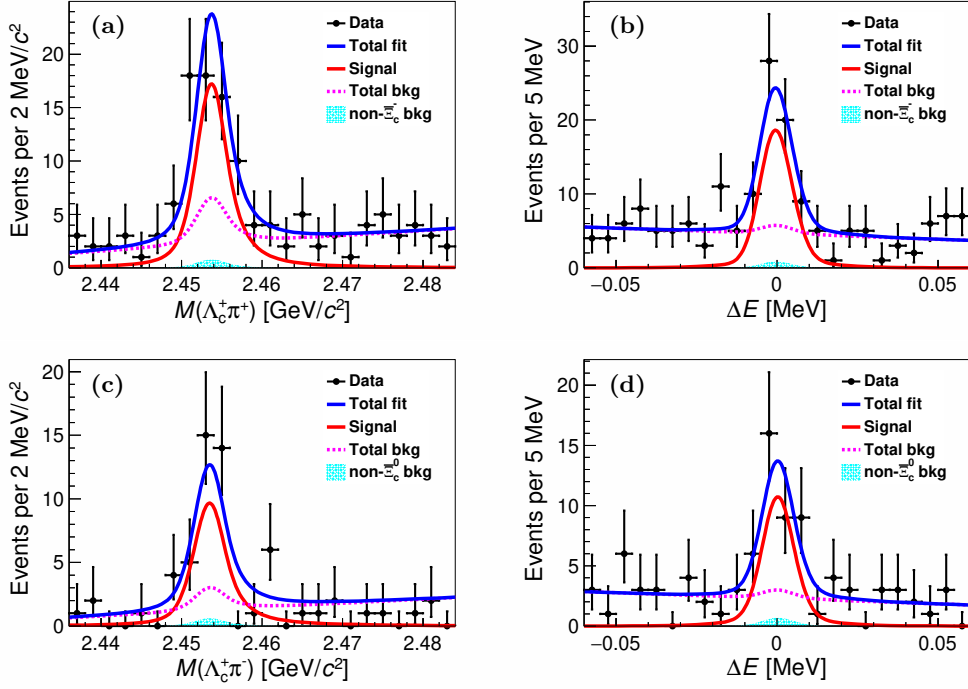


FIG. 2: Distributions of (a, c) $M(\Lambda_c^+ \pi^\pm)$ and (b, d) ΔE for the reconstructed (top) $B^+ \rightarrow \Sigma_c(2455)^{++} \Xi_c^-$ and (bottom) $B^0 \rightarrow \Sigma_c(2455)^0 \Xi_c^-$ candidates, using events from the signal regions of $M(\Xi_c^-)$ in the combined Belle and Belle II data sets. Points with error bars are the data, the solid blue curves show the total fit results, the solid red curves correspond to the fitted signal components, and the dashed magenta curves represent the total fitted background components. The shaded cyan regions show the peaking-background contributions from the inclusive $B^{+,0} \rightarrow \Sigma_c(2455)^{+,0} X$ decays, where $X \neq \Xi_c^-$.

$\Sigma_c(2455)^{++} \Xi_c^-$ or $B^0 \rightarrow \Sigma_c(2455)^0 \Xi_c^-$ signal events in the combined Belle and Belle II data sets; $N_{\Upsilon(4S)}^{b1,b2}$ denotes the total number of $\Upsilon(4S)$ events in the Belle or Belle II data sets; f_x refers to the fraction of charged (f_{+-}) or neutral (f_{00}) $B\bar{B}$ pairs [48]; the term $\sum_i (\varepsilon_i^{b1,b2} \mathcal{B}_i)$ represents the sum over all reconstruction modes ($i = 1 - 4$) of the products of reconstruction efficiencies $\varepsilon_i^{b1,b2}$ (for Belle or Belle II) and the corresponding secondary branching fractions \mathcal{B}_i . The numerical values of the above quantities and the calculated branching fractions are summarized in Table I. The branching fractions measured separately in Belle and Belle II data are examined and found to be consistent with the results from simultaneous fits within 1σ .

We consider several source of systematic uncertainties, including detection-efficiency-related (DER) uncertainties (σ_{DER}), the statistical uncertainty on the efficiency determined from simulation (σ_{eff}), the uncertainties on the branching fractions of intermediate states ($\sigma_{\mathcal{B}_i}$), the uncertainty on the total number of $\Upsilon(4S)$ events ($\sigma_{N_{\Upsilon(4S)}}$), the uncertainty on the fraction of charged or neutral $B\bar{B}$ events (σ_{f_x}), the possible correlation between the $M(\Lambda_c^+ \pi^\pm)$ versus ΔE distributions (σ_{corr}), and uncertainties associated with the fit models (σ_{fit}). Table II summarizes these

systematic uncertainties, with the total uncertainty (σ_{total}) calculated as the quadratic sum of the uncertainties from each source.

The DER uncertainties include those from tracking efficiency, PID efficiency, and the reconstructions of K_S^0 and Λ candidates, which are estimated using data control samples. The uncertainty associated with tracking efficiency depends on the particle charge, momentum and polar angle, and ranges from 0.31% to 0.91% (0.38% to 1.07%) for each track at Belle (Belle II), as determined from the data control samples described in Ref. [49]. The slightly larger tracking uncertainties in Belle II result from the limited statistics of the control samples used. The PID efficiency uncertainties are estimated to be 1.0% (0.8%) for pion, 1.3% (1.0%) for kaon, and 2.4% (1.8%) for proton at Belle (Belle II) [43, 44]. The K_S^0 reconstruction uncertainty is evaluated to be 1.2% (1.9%) at Belle (Belle II), and the Λ reconstruction uncertainty is estimated to be 2.3% (2.1%). Both are obtained following the procedure of Ref. [49]. The individual uncertainties of the different modes at Belle and Belle II are summed and weighted by $N_{\Upsilon(4S)}^{b1,b2} (\varepsilon_i^{b1,b2} \mathcal{B}_i)$. Assuming these uncertainties are independent and adding them in quadrature, the detection-efficiency-related uncertainties are evaluated to be 2.6% for $B^+ \rightarrow \Sigma_c(2455)^{++} \Xi_c^-$ decay

TABLE I: Summary of analysis inputs and fit results. We list only the statistical uncertainties of the signal yields. For the branching fractions, the first and second uncertainties are statistical and systematic, respectively, while the third originates from the absolute branching fractions of $\Xi_c^{-,0}$ decays [1].

	N_{ss}^{sig}	$N_{\Upsilon(4S)}^{b1} (10^6)$	$N_{\Upsilon(4S)}^{b2} (10^6)$	f_x	$\sum_i (\varepsilon_i^{b1} \mathcal{B}_i) (10^{-5})$	$\sum_i (\varepsilon_i^{b2} \mathcal{B}_i) (10^{-5})$	$\mathcal{B} (10^{-4})$
B^+	52.8 ± 10.2	772	387	0.5113	7.1	9.1	$5.74 \pm 1.11 \pm 0.42_{-1.53}^{+2.47}$
B^0	31.1 ± 7.2	772	387	0.4861	5.2	6.8	$4.83 \pm 1.12 \pm 0.37_{-0.60}^{+0.72}$

and 2.2% for $B^0 \rightarrow \Sigma_c(2455)^0 \Xi_c^0$ decay. A study of the control samples $B^+ \rightarrow \Lambda_c^+ \Xi_c^-$ and $B^0 \rightarrow \Lambda_c^+ \Xi_c^-$, which have topologies similar to the signal channels, indicates that the differences in vertex fit efficiencies for intermediate particles between data and simulation are negligible.

The statistical uncertainty of simulation-based efficiency is at most 1.0%. The relative uncertainties of the absolute branching fractions of $\Lambda_c^+ \rightarrow p K^- \pi^+$, $\Lambda_c^+ \rightarrow p K_S^0$, $K_S^0 \rightarrow \pi^+ \pi^-$, $\Xi_c^- \rightarrow \Xi^+ \pi^- \pi^-$, $\Xi_c^- \rightarrow \bar{p} K^+ \pi^-$, $\Xi_c^0 \rightarrow \Xi^+ \pi^-$, $\Xi_c^0 \rightarrow \bar{\Lambda} K^+ \pi^-$, $\Xi^+ \rightarrow \bar{\Lambda} \pi^+$, and $\bar{\Lambda} \rightarrow \bar{p} \pi^+$ are taken from Ref. [1]. Since the large uncertainties in the branching fractions of the intermediate decays $\Xi_c^- \rightarrow \Xi^+ \pi^- \pi^-$ (44.8%), $\Xi_c^- \rightarrow \bar{p} K^+ \pi^-$ (48.4%), $\Xi_c^0 \rightarrow \Xi^+ \pi^-$ (18.9%), and $\Xi_c^0 \rightarrow \bar{\Lambda} K^+ \pi^-$ (19.3%) might be reduced with future measurements, we treat them separately as a third source of uncertainty. The branching fraction of each intermediate state is varied independently by $\pm 1\sigma$, with the resulting deviation from the nominal value taken as the corresponding systematic uncertainty. There are uncertainties of $^{+43\%}_{-27\%}$, $^{+15\%}_{-12\%}$, and 4.0% associated with the absolute branching fractions of Ξ_c^- , Ξ_c^0 , and other intermediate states, respectively. The uncertainties of $N_{\Upsilon(4S)}^{b1,b2}$ are 1.4% for Belle [50] and 1.5% for Belle II [51], and are combined into a total uncertainty weighted by $N_{\Upsilon(4S)}^{b1,b2} \sum_i (\varepsilon_i^{b1,b2} \mathcal{B}_i)$. The uncertainties of f_{+-} and f_{00} are 2.1% and 1.7% [48], respectively. The uncertainty arising from the possible correlation between the $M(\Lambda_c^+ \pi^\pm)$ and ΔE distributions is estimated using a bootstrap method [52]. A total of 500 bootstrap samples are constructed from the simulated samples. For each bootstrap sample, the signal and background yields are generated by sampling from Poisson distributions centered at the values obtained from the fit to data. The deviation between the mean of the output signal yield distribution and the central value used in the generation is taken as the systematic uncertainty.

The systematic uncertainties associated with the fit models arise from the empirical choice of background PDFs, the mass resolution differences between data and simulation, the fixed width of $\Sigma_c(2455)^{+,0}$, and the choice of sideband regions for $M(\Xi_c^{-,0})$. To estimate the uncertainty due to the background parametrization, the nominal background PDFs $b_1(M)$ and $b_2(\Delta E)$

are replaced with either second-order polynomials or exponential functions, and the largest deviation from the nominal fit result is assigned as the systematic uncertainty. The uncertainty due to mass-resolution differences between data and simulation is assessed by convolving the fixed signal shapes $s_1(M)$ and $s_2(\Delta E)$ with Gaussian functions having free widths, and the resulting deviation from the nominal fit is taken as the corresponding uncertainty. The effect of the fixed width of $\Sigma_c(2455)^{+,0}$ is evaluated by varying each width by $\pm 1\sigma$ [1], and assigning the largest deviation as the systematic uncertainty. The sideband regions of $M(\Xi_c^{-,0})$ are shifted by $\pm 10 \text{ MeV}/c^2$, and the largest resulting deviation is taken as the corresponding systematic uncertainty. All of these contributions are summed in quadrature to obtain the total systematic uncertainty related to the fit models.

TABLE II: Summary of fractional systematic uncertainties (%).

	σ_{DER}	σ_{eff}	$\sigma_{\mathcal{B}_i}$	$\sigma_{N_{\Upsilon(4S)}}$	σ_{f_x}	σ_{corr}	σ_{fit}	σ_{total}
B^+	2.6	1.0	4.0	1.1	2.1	2.2	4.4	7.3
B^0	2.2	1.0	4.0	1.1	1.7	2.7	5.2	7.8

In summary, we report the first observation of the two-body baryonic decays $B^+ \rightarrow \Sigma_c(2455)^{++} \Xi_c^-$ and $B^0 \rightarrow \Sigma_c(2455)^0 \Xi_c^0$, using electron-positron data samples that contain 772×10^6 and 387×10^6 $\Upsilon(4S)$ events collected by the Belle and Belle II detectors, respectively. The branching fractions are measured to be $\mathcal{B}(B^+ \rightarrow \Sigma_c(2455)^{++} \Xi_c^-) = (5.74 \pm 1.11 \pm 0.42_{-1.53}^{+2.47}) \times 10^{-4}$ and $\mathcal{B}(B^0 \rightarrow \Sigma_c(2455)^0 \Xi_c^0) = (4.83 \pm 1.12 \pm 0.37_{-0.60}^{+0.72}) \times 10^{-4}$, where the uncertainties are statistical, systematic, and from the absolute branching fractions of Ξ_c^- or Ξ_c^0 decays, respectively. The observed branching fractions are an order of magnitude smaller than those predicted by the QCD sum rule [17], but are consistent with the expectations of the diquark model [18]. Interestingly, these branching fractions are larger than those of their singly-charmed counterparts, $B^+ \rightarrow \bar{\Sigma}_c(2455)^0 p$ and $B^0 \rightarrow \bar{\Sigma}_c(2455)^- p$, by one to two orders of magnitude [1], although the corresponding combinations of CKM matrix elements in their amplitudes have nearly equal magnitudes.

We are grateful to Professors Yu-Kuo Hsiao, Hai-Yang

Cheng, and Ying Li for their insightful comments and valuable suggestions. This work, based on data collected using the Belle II detector, which was built and commissioned prior to March 2019, and data collected using the Belle detector, which was operated until June 2010, was supported by Higher Education and Science Committee of the Republic of Armenia Grant No. 23LCG-1C011; Australian Research Council and Research Grants No. DP200101792, No. DP210101900, No. DP210102831, No. DE220100462, No. LE210100098, and No. LE230100085; Austrian Federal Ministry of Education, Science and Research, Austrian Science Fund (FWF) Grants DOI: 10.55776/P34529, DOI: 10.55776/J4731, DOI: 10.55776/J4625, DOI: 10.55776/M3153, and DOI: 10.55776/PAT1836324, and Horizon 2020 ERC Starting Grant No. 947006 “InterLeptons”; Natural Sciences and Engineering Research Council of Canada, Compute Canada and CANARIE; National Key R&D Program of China under Contract No. 2024YFA1610503, and No. 2024YFA1610504 National Natural Science Foundation of China and Research Grants No. 11575017, No. 11761141009, No. 11705209, No. 11975076, No. 12135005, No. 12150004, No. 12161141008, No. 12475093, and No. 12175041, China Postdoctoral Science Foundation (CPSF) under Grant No. 2024M760485, and China Postdoctoral Fellowship Program of CPSF under Grant No. GZC20240303, and Shandong Provincial Natural Science Foundation Project ZR2022JQ02; the Czech Science Foundation Grant No. 22-18469S, Regional funds of EU/MEYS: OPJAK FORTE CZ.02.01.01/00/22_008/0004632 and Charles University Grant Agency project No. 246122; European Research Council, Seventh Framework PIEF-GA-2013-622527, Horizon 2020 ERC-Advanced Grants No. 267104 and No. 884719, Horizon 2020 ERC-Consolidator Grant No. 819127, Horizon 2020 Marie Skłodowska-Curie Grant Agreement No. 700525 “NIOBE” and No. 101026516, and Horizon 2020 Marie Skłodowska-Curie RISE project JENNIFER2 Grant Agreement No. 822070 (European grants); L’Institut National de Physique Nucléaire et de Physique des Particules (IN2P3) du CNRS and L’Agence Nationale de la Recherche (ANR) under Grant No. ANR-21-CE31-0009 (France); BMFTR, DFG, HGF, MPG, and AvH Foundation (Germany); Department of Atomic Energy under Project Identification No. RTI 4002, Department of Science and Technology, and UPES SEED funding programs No. UPES/R&D-SEED-INFRA/17052023/01 and No. UPES/R&D-SOE/20062022/06 (India); Israel Science Foundation Grant No. 2476/17, U.S.-Israel Binational Science Foundation Grant No. 2016113, and Israel Ministry of Science Grant No. 3-16543; Istituto Nazionale di Fisica Nucleare and the Research Grants BELLE2, and the ICSC – Centro Nazionale di Ricerca in High Performance Computing, Big Data and Quantum Computing, funded by European Union – NextGenerationEU; Japan

Society for the Promotion of Science, Grant-in-Aid for Scientific Research Grants No. 16H03968, No. 16H03993, No. 16H06492, No. 16K05323, No. 17H01133, No. 17H05405, No. 18K03621, No. 18H03710, No. 18H05226, No. 19H00682, No. 20H05850, No. 20H05858, No. 22H00144, No. 22K14056, No. 22K21347, No. 23H05433, No. 26220706, and No. 26400255, and the Ministry of Education, Culture, Sports, Science, and Technology (MEXT) of Japan; National Research Foundation (NRF) of Korea Grants No. 2021R1-F1A-1064008, No. 2022R1-A2C-1003993, No. 2022R1-A2C-1092335, No. RS-2016-NR017151, No. RS-2018-NR031074, No. RS-2021-NR060129, No. RS-2023-00208693, No. RS-2024-00354342 and No. RS-2025-02219521, Radiation Science Research Institute, Foreign Large-Size Research Facility Application Supporting project, the Global Science Experimental Data Hub Center, the Korea Institute of Science and Technology Information (K25L2M2C3) and KREONET/GLORIAD; Universiti Malaya RU grant, Akademi Sains Malaysia, and Ministry of Education Malaysia; Frontiers of Science Program Contracts No. FOINS-296, No. CB-221329, No. CB-236394, No. CB-254409, and No. CB-180023, and SEP-CINVESTAV Research Grant No. 237 (Mexico); the Polish Ministry of Science and Higher Education and the National Science Center; the Ministry of Science and Higher Education of the Russian Federation and the HSE University Basic Research Program, Moscow; University of Tabuk Research Grants No. S-0256-1438 and No. S-0280-1439 (Saudi Arabia), and Researchers Supporting Project number (RSPD2025R873), King Saud University, Riyadh, Saudi Arabia; Slovenian Research Agency and Research Grants No. J1-50010 and No. P1-0135; Ikerbasque, Basque Foundation for Science, State Agency for Research of the Spanish Ministry of Science and Innovation through Grant No. PID2022-136510NB-C33, Spain, Agencia Estatal de Investigación, Spain Grant No. RYC2020-029875-I and Generalitat Valenciana, Spain Grant No. CIDEGENT/2018/020; the Swiss National Science Foundation; The Knut and Alice Wallenberg Foundation (Sweden), Contracts No. 2021.0174 and No. 2021.0299; National Science and Technology Council, and Ministry of Education (Taiwan); Thailand Center of Excellence in Physics; TUBITAK ULAKBIM (Turkey); National Research Foundation of Ukraine, Project No. 2020.02/0257, and Ministry of Education and Science of Ukraine; the U.S. National Science Foundation and Research Grants No. PHY-1913789 and No. PHY-2111604, and the U.S. Department of Energy and Research Awards No. DE-AC06-76RLO1830, No. DE-SC0007983, No. DE-SC0009824, No. DE-SC0009973, No. DE-SC0010007, No. DE-SC0010073, No. DE-SC0010118, No. DE-SC0010504, No. DE-SC0011784, No. DE-SC0012704, No. DE-SC0019230, No. DE-SC0021274, No. DE-SC0021616, No. DE-SC0022350, No. DE-SC0023470; and the Vietnam Academy of Science and Technology

(VAST) under Grants No. NVCC.05.12/22-23 and No. DL0000.02/24-25.

These acknowledgements are not to be interpreted as an endorsement of any statement made by any of our institutes, funding agencies, governments, or their representatives.

We thank the SuperKEKB team for delivering high-

luminosity collisions; the KEK cryogenics group for the efficient operation of the detector solenoid magnet and IBBelle on site; the KEK Computer Research Center for on-site computing support; the NII for SINET6 network support; and the raw-data centers hosted by BNL, DESY, GridKa, IN2P3, INFN, PNNL/EMSL, and the University of Victoria.

-
- [1] S. Navas *et al.* (Particle Data Group), Phys. Rev. D **110**, 030001 (2024).
 - [2] K. Abe *et al.* (Belle Collaboration), Phys. Rev. Lett. **88**, 181803 (2002).
 - [3] M. Z. Wang *et al.* (Belle Collaboration), Phys. Rev. Lett. **92**, 131801 (2004).
 - [4] B. Aubert *et al.* (BaBar Collaboration), Phys. Rev. D **72**, 051101 (2005).
 - [5] R. Aaij *et al.* (LHCb Collaboration), Phys. Rev. D **96**, 051103 (2017).
 - [6] R. Chistov, J. Phys. Conf. Ser. **675**, 022007 (2016).
 - [7] X. Huang, Y. K. Hsiao, J. Wang, and L. Sun, Adv. High Energy Phys. **2022**, 4343824 (2022).
 - [8] Ed. A. J. Bevan, B. Golob, Th. Mannel, S. Prell, and B. D. Yabsley, Eur. Phys. J. C **74**, 3026 (2014).
 - [9] N. Gabyshev *et al.* (Belle Collaboration), Phys. Rev. Lett. **90**, 121802 (2003).
 - [10] R. Chistov *et al.* (Belle Collaboration), Phys. Rev. D **74**, 111105 (2006).
 - [11] B. Aubert *et al.* (BaBar Collaboration), Phys. Rev. D **77**, 031101 (2008).
 - [12] H. Y. Cheng, Int. J. Mod. Phys. A **21**, 4209 (2006).
 - [13] H. Y. Cheng, C. K. Chua, and S. Y. Tsai, Phys. Rev. D **73**, 074015 (2006).
 - [14] H. Y. Cheng, C. K. Chua, and Y. K. Hsiao, Phys. Rev. D **79**, 114004 (2009).
 - [15] C. H. Chen, Phys. Lett. B **638**, 214 (2006).
 - [16] Z. Rui, Z. T. Zou, and Y. Li, J. High Energy Phys. **12**, 159 (2024).
 - [17] V. L. Chernyak and I. R. Zhitnitsky, Nucl. Phys. B **345**, 137 (1990).
 - [18] P. Ball and H. G. Dosch, Z. Phys. C **51**, 445 (1991).
 - [19] Y. K. Hsiao, J. High Energy Phys. **11**, 117 (2023).
 - [20] H. Y. Cheng, Nucl. Phys. B Proc. Suppl. **163**, 68 (2007).
 - [21] R. C. Verma, Phys. Lett. B **365**, 377 (1996).
 - [22] A. C. Katoch, K. K. Sharma, and R. C. Verma, J. Phys. G **23**, 807 (1997).
 - [23] A. N. Kamal, A. B. Santra, T. Uppal, and R. C. Verma, Phys. Rev. D **53**, 2506 (1996).
 - [24] M. Kaur and R. C. Verma, J. Subatomic Part. Cosmol. **3**, 100033 (2025).
 - [25] J. Brodzicka *et al.* (Belle Collaboration), Prog. Theor. Exp. Phys. **2012**, 04D001 (2012).
 - [26] A. Abashian *et al.* (Belle Collaboration), Nucl. Instrum. Meth. A **479**, 117 (2002).
 - [27] I. Adachi *et al.* (Belle Collaboration), Chin. Phys. C **49**, 013001 (2025).
 - [28] T. Abe *et al.* (Belle II Collaboration), arXiv:1011.0352.
 - [29] G. Punzi, eConf C030908, MODT002 (2003).
 - [30] S. Kurokawa and E. Kikutani, Nucl. Instrum. Meth. A **499**, 1 (2003), and other papers included in this volume; T. Abe *et al.*, Prog. Theor. Exp. Phys. **2013**, 03A001 (2013), and references therein.
 - [31] K. Akai *et al.* (SuperKEKB Accelerator Team), Nucl. Instrum. Meth. A **907**, 188 (2018).
 - [32] D. J. Lange, Nucl. Instrum. Meth. A **462**, 152 (2001).
 - [33] T. Sjostrand, S. Mrenna, and P. Z. Skands, J. High Energy Phys. **05**, 026 (2006).
 - [34] T. Sjöstrand *et al.*, Comput. Phys. Commun. **191**, 159 (2015).
 - [35] E. Barberio, B. van Eijk, and Z. Was, Comput. Phys. Commun. **66**, 115 (1991).
 - [36] X. Y. Zhou, S. X. Du, G. Li, and C. P. Shen, Comput. Phys. Commun. **258**, 107540 (2021).
 - [37] S. Jachad, B. F. L. Ward, and Z. Was, Comput. Phys. Commun. **130**, 260 (2000).
 - [38] R. Brun *et al.*, GEANT3: user's guide Geant 3.10, Geant 3.11, CERN Report No. DD/EE/84-1, 1984.
 - [39] S. Agostinelli *et al.* (GEANT4 Collaboration), Nucl. Instrum. Meth. A **506**, 250 (2003).
 - [40] T. Kuhr, C. Pulvermacher, M. Ritter, T. Hauth, and N. Braun (Belle II Framework Software Group), Comput. Softw. Big Sci. **3**, 1 (2019).
 - [41] <https://doi.org/10.5281/zenodo.5574115>.
 - [42] M. Gelb *et al.* Comput. Softw. Big Sci. **2**, 9 (2018).
 - [43] E. Nakano, Nucl. Instrum. Meth. A **494**, 402 (2002).
 - [44] I. Adachi *et al.* (Belle II Collaboration), arXiv:2506.04355.
 - [45] H. Nakano *et al.* (Belle Collaboration) Phys. Rev. D **97**, 092003 (2018).
 - [46] F. Abudinén *et al.* (Belle and Belle II Collaborations), J. High Energy Phys. **02**, 063 (2022).
 - [47] See the supplemental material for the $M(\Lambda_c^+ \pi^\pm)$ and ΔE distributions from the sideband regions.
 - [48] S. Banerjee *et al.* (Heavy Flavor Averaging Group), arXiv:2411.18639.
 - [49] I. Adachi *et al.* (Belle and Belle II Collaborations), J. High Energy Phys. **03**, 061 (2025).
 - [50] S. Watanuki *et al.* (Belle Collaboration) Phys. Rev. Lett. **130**, 261802 (2023).
 - [51] I. Adachi *et al.* (Belle and Belle II Collaborations), Phys. Rev. D **110**, L031106 (2024).
 - [52] B. Efron, Annals Statist. **7**, 1 (1979).

Supplemental Material for “Observation of the decays $B^+ \rightarrow \Sigma_c(2455)^{++}\Xi_c^-$ and $B^0 \rightarrow \Sigma_c(2455)^0\Xi_c^0$ ”

$M(\Lambda_c^+\pi^\pm)$ and ΔE distributions: Figures 1 and 2 show the $M(\Lambda_c^+\pi^\pm)$ and ΔE distributions derived from the sideband regions of $M(\Lambda_c^+)$ and M_{bc} for the $B^+ \rightarrow \Sigma_c(2455)^{++}\Xi_c^-$ and $B^0 \rightarrow \Sigma_c(2455)^0\Xi_c^0$ decays, respectively, in the combined Belle and Belle II data sets.

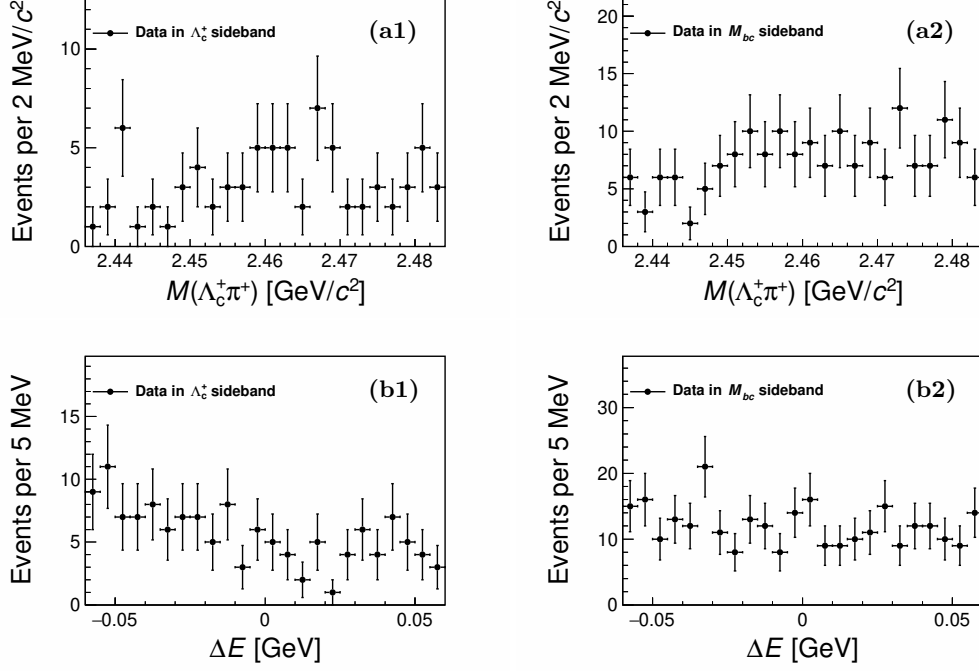


FIG. 1: Distributions of (a) $M(\Lambda_c^+\pi^\pm)$ and (b) ΔE from the sideband regions of (1) $M(\Lambda_c^+)$ and (2) M_{bc} for the $B^+ \rightarrow \Sigma_c(2455)^{++}\Xi_c^-$ decay in the combined Belle and Belle II data sets.

Fit results to the $M(\Lambda_c^+\pi^\pm)$ and ΔE distributions from the sideband regions of $M(\Xi_c^-,0)$: Figure 3 shows the fit results to the $M(\Lambda_c^+\pi^\pm)$ and ΔE distributions from the sideband regions of $M(\Xi_c^-,0)$ in the combined Belle and Belle II data sets.

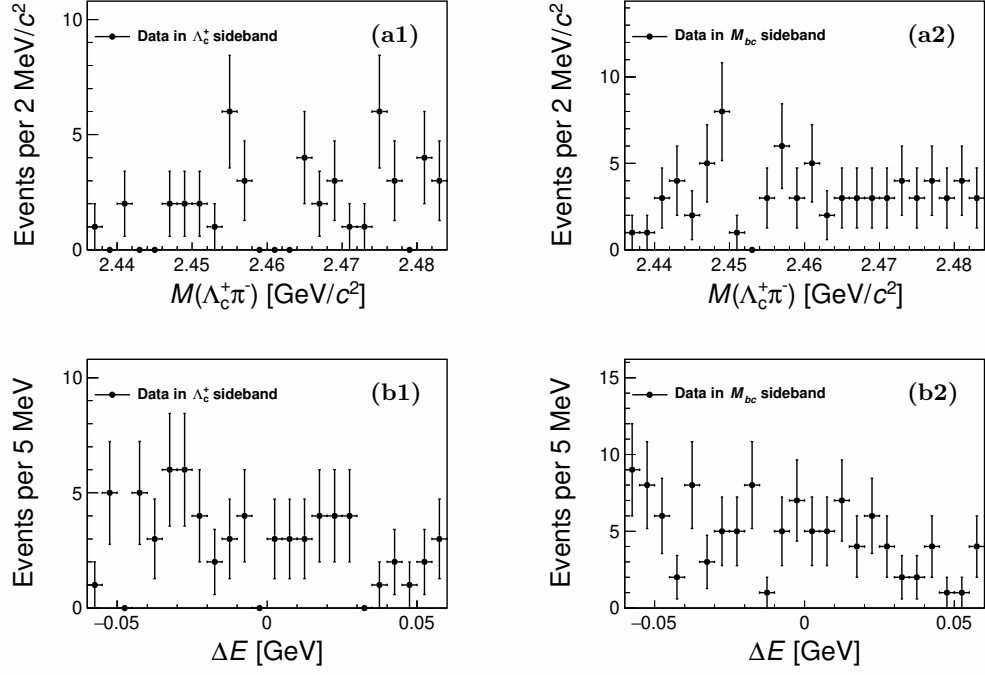


FIG. 2: Distributions of (a) $M(\Lambda_c^+ \pi^+)$ and (b) ΔE from the sideband regions of (1) $M(\Lambda_c^+)$ and (2) M_{bc} for the $B^0 \rightarrow \Sigma_c(2455)^0 \Xi_c^{0-}$ decay in the combined Belle and Belle II data sets.

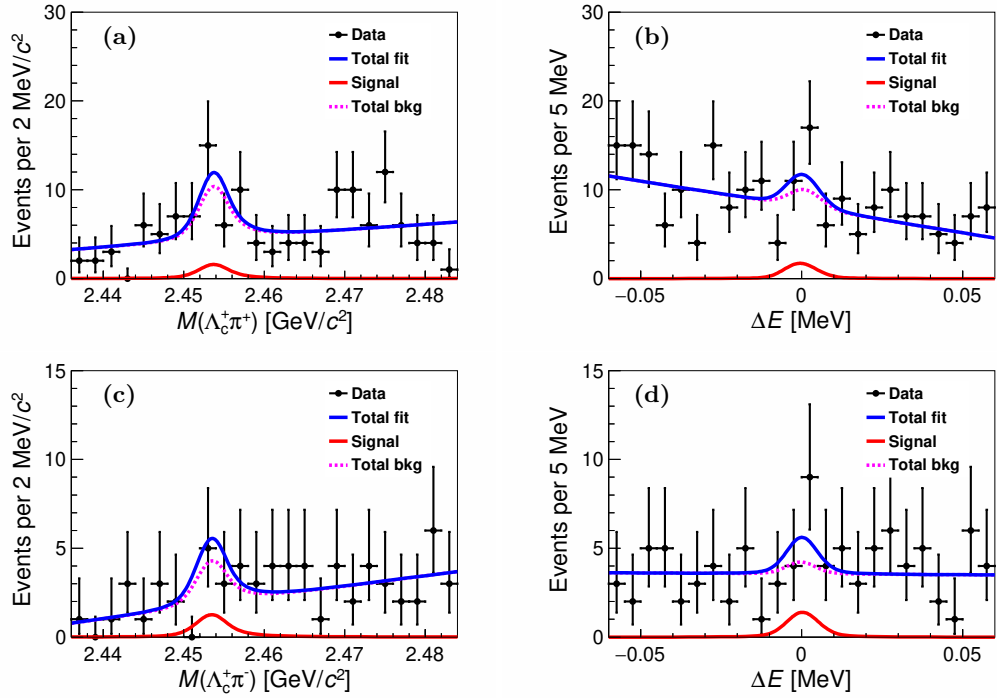


FIG. 3: Distributions of (a, c) $M(\Lambda_c^+ \pi^+)$ and (b, d) ΔE for the reconstructed (top) $B^+ \rightarrow \Sigma_c(2455)^{++} \Xi_c^-$ and (bottom) $B^0 \rightarrow \Sigma_c(2455)^0 \Xi_c^{0-}$ candidates, using events from the sideband regions of $M(\Xi_c^{0-})$ in the combined Belle and Belle II data sets. All components are indicated in the legends.